

An overall optimization and solution framework for urban historical and future DRIF under climate change

XingChen Ding^{a,b}, WeiHong Liao^{c,*}, Hao Wang^d, Hao Wang^c, XiaoHui Lei^c and JiaLi Yang^e

^a College of Resources and Civil Engineering, Northeastern University, Shenyang 110819, China

^b Science and Technology Innovation Center of Smart Water and Resource Environment, Northeastern University, Shenyang 110819, China

^c State Key Laboratory of Simulation and Regulation of Water Cycle in River Basin, China Institute of Water Resources and Hydropower Research, Beijing 100038, China

^d Faculty of Architecture, Civil and Transportation Engineering, Beijing University of Technology, Beijing 100124, China

^e School of Hydropower and Information Engineering, Huazhong University of Science and Technology, Wuhan 430074, China

*Corresponding author. E-mail: behellen@163.com

ABSTRACT

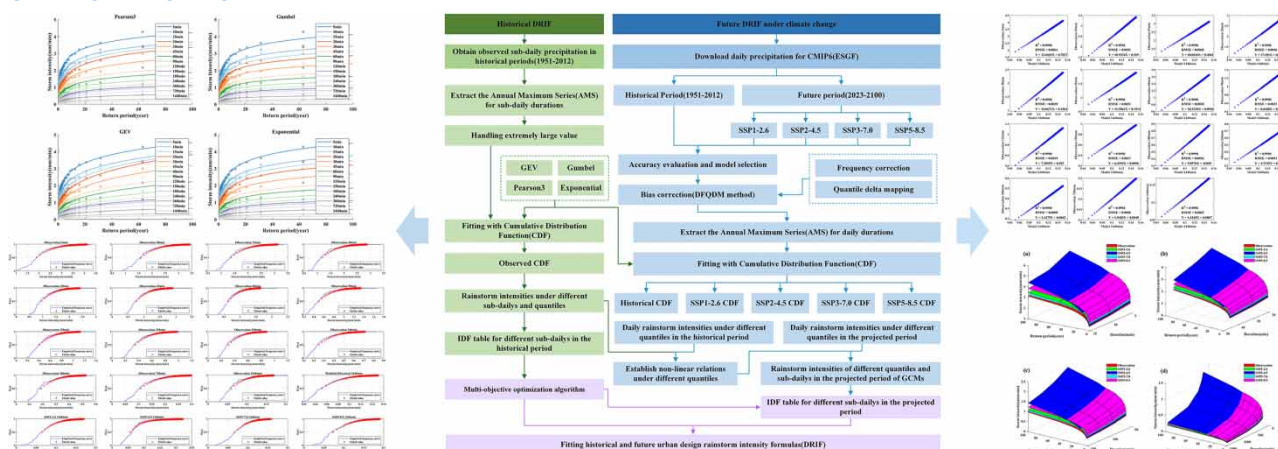
The estimation and application of Intensity-Duration-Frequency (IDF) curves depend on the assumption of stationarity of the rainfall series, which is that the intensity and frequency of extreme hydrological events remain unchanged in the future. Climate change will have a significant impact on the collection and utilization of rainwater and its spatial characteristics. When the Gray-Green infrastructure is designed, if only historical precipitation is adopted to calculate the urban design rainstorm intensity formula (DRIF) and the total annual runoff control rate, it may be difficult to meet the demand of future precipitation changes on the city's ability to accommodate rainfall. Therefore, it is very important to study the impact of climate change on the IDF curve. This study proposes an overall optimization solution framework for historical and future DRIF. The impact of the extreme value on the IDF curve during the historical period is analyzed. The calculation method of the IDF curve in the future period is established. The changes of the rainstorm intensity in the historical and future period (SSP1-2.6, SSP2-4.5, SSP3-7.0, SSP5-8.5) were analyzed for the 15 durations and eight return periods in Beijing, China. The results of this study show that the nondominated sorting and local search (NSLS) has the best accuracy in fitting the statistical samples of precipitation for different durations. The best methods to judge and process the extreme value of the statistical sample are Z-score and average value of series greater than critical value (AVG). Under the four SSP scenarios, the estimated IDF value is larger than the observed value in the historical period. The results of the equivalent return period calculated using the DRIF show that the the four SSP scenarios are smaller than the historical period for the return period greater than five years. Taking 120 min of short-duration precipitation as an example, the 100-year equivalent return periods of the observation under the four SSP scenarios are 35-, 20-, 54-, and 17-years, respectively. The research can provide valuable reference for the design and planning of the drainage facility under climate change.

Key words: climate change, CMIP6, equivalent return period, extreme precipitation, IDF, outliers

HIGHLIGHTS

- The best methods to judge and process the extreme value of IDF are Z-Score and average value of series greater than critical value (AVG).
- Under the four SSP (SSP1-2.6, SSP2-4.5, SSP3-7.0, SSP5-8.5) scenarios, the estimated IDF value is larger than the observed value in the historical period.

GRAPHICAL ABSTRACT



1. INTRODUCTION

As one of the most sensitive and vulnerable areas affected by climate change, extreme weather and disaster events occur frequently in China. Geological disasters such as urban waterlogging, farmland waterlogging, mountain torrents and mudslides caused by heavy rainfall have caused serious influence to people's production and life. With regard to the future global climate change, the fifth assessment report of the IPCC (Intergovernmental Panel on Climate Change) indicated that evolutions in precipitation and melting of snow and ice in many regions are changing the hydrological system, affecting the quantity and quality of water resources (medium confidence) (Pachauri *et al.* 2014). From 1880 to 2012, the global average temperature increased by 0.85 °C (Zhang *et al.* 2021). Under the influence of climate change, glaciers close to the global scale are shrinking continuously (high confidence), affecting the downstream runoff and water resources (medium confidence). Climate change is causing warming and thawing of permafrost at high latitudes and altitudes (high confidence). The extreme weather and climate events caused by the impact of human activities include the decrease of low-temperature extreme events, the increase of high-temperature extreme events, the increase of extremely high sea levels and the increase of the number of heavy precipitation events in some regions. The number of heavy precipitation events may show an increasing trend in more land areas than in areas with decreased precipitation. All the emission scenarios evaluated predict that the surface temperature will increase in the 21st century. The frequency of heat wave is likely to be higher and longer, and the intensity and frequency of extreme precipitation in many areas will increase. The oceans will continue to heat up and acidify, and the global average sea level will also continue to rise. The results of the above analysis show that the probability and frequency of extreme weather will have a significant increasing trend for a long period in the future, which brings great challenges to countries around the world to deal with disastrous weather.

The design rainstorm intensity formula (DRIF) is an important basis for reflecting the regularity of rainfall, guiding the design of urban drainage and waterlogging prevention projects and the construction of related facilities. The accuracy of its calculation has an important impact on the project cost, drainage capacity, people's property and life safety (Mirhosseini *et al.* 2013; Fadhel *et al.* 2017). The rainstorm intensity of short-duration heavy precipitation becomes larger under climate change. Compared with the original DRIF, the precipitation for the same return period and the duration will increase. The original DRIF can no longer meet the design requirements of future projects.

The DRIF is obtained by fitting the intensity-duration-frequency (IDF) curves. The IDF assumes that the historical precipitation is stationary, so it can be used to characterize future changes in extreme precipitation. When climatic conditions change rapidly, IDF curves generated only based on historical data will erroneously represent future climate changes (Mailhot *et al.* 2007; Srivastav *et al.* 2014). In urban hydrology, the design of drainage infrastructure has traditionally been based on statistical analysis of historical precipitation records. It is assumed that the intensity and frequency of past events are statistically representative of what may happen in the near future. However, in the context of climate change, the assumption must be revisited and design criteria for drainage infrastructure revised to account for expected changes in the intensity

and frequency of heavy rainfall. Otherwise, it will have a serious impact on the future design, operation and maintenance of drainage facilities (Mailhot *et al.* 2007; Tfwala *et al.* 2017).

Considering the increase of observed heavy rainfall events, IDF curves should be updated to take into account the changing climate, especially for the design of urban infrastructure. Beijing is the capital of China, with complex terrain, high population concentration, and severe rainstorms (Lu & Cui 2022). For example, in 2012 and 2016, Beijing experienced torrential rains on July 20th and July 21st, respectively, which caused severe urban waterlogging and massive economic losses. To the best of our knowledge, there are currently no studies evaluating the impact of climate change on the IDF curve in Beijing. Few studies have calculated future DRIF based on IDF curves under climate change. At present, the research on IDF curve mainly has the following problems: (1) When the extreme value of sub-daily precipitation in one year is much higher than that in other years, it will lead to poor fitting effect of the tail of the frequency distribution curve. Overfitting to the tail will result in smaller rainstorm intensity for the fitting of head; (2) For the calculation of future IDF, many studies have modified the historical IDF curve to obtain the future IDF according to the proportion of rainstorm intensity values in different return periods of future and historical climate models. This solution method using proportional increments does not consider the correlation between future IDF and observed values.

The objectives of this study are as follows: (1) Based on the minute-level precipitation data, the influence of this extreme value on the shape and fitting accuracy of the historical frequency distribution curve is analyzed; (2) The calculation process of future IDF curve based on the Coupled Model Intercomparison Project Phase 6 (CMIP6) is given; (3) The variation of the equivalent return period before and after climate change is analyzed; (4) The historical and future DRIFs of Beijing under climate change are calculated. This research can provide a reference for the planning and design of water resources projects in Beijing or other areas in the future.

2. STUDY AREA AND DATA SERIES

2.1. Study area

Beijing is the capital of China and one of the most populous cities in the world (Song *et al.* 2019; Xu *et al.* 2022). It is located at the northern tip of the North China Plain (Figure 1). The metropolitan area of Beijing has a total area of 16,410 km² and has a complex topography (Song *et al.* 2014). Beijing is located in the transitional zone between mountains and plains, with 62% of the mountains and 38% of the plains (Jia *et al.* 2017). The annual average temperature ranges from 11 to 13 °C. The average annual precipitation in Beijing is 508.8 mm/year from 2001 to 2015 (Ren *et al.* 2018). Beijing has a typical monsoon-driven semi-humid to humid continental climate. It is hot and humid in summer and cold and dry in winter. The number of rainfall days and precipitation in Beijing is mainly concentrated in summer, accounting for about two-thirds of the total annual precipitation (Yang *et al.* 2019).

2.2. Data series

The minute-level precipitation for the observation comes from the Guanxiangtai Weather Station in Beijing, the range of which is from 1951 to 2012. CMIP6 was adopted as projected precipitation for future climate change analysis. Its range includes historical periods (1951–2012) and future periods (2023–2100). In this study 12 models were selected for accuracy evaluation, which are listed in Table 1. The results of this evaluation show that the accuracy of CanESM5 is the best. The PBIAS and RMSE of CanESM5 are the smallest for annual precipitation, which are −7.33 and 239.66, respectively. The trend of the change is more consistent with the observed value. The CC of CanESM5 and the observed monthly precipitation is 0.59. CanESM5 is chosen to describe changes in precipitation for future period. The process of evaluation and selection for CMIP6 is not described in detail in this study. For the method of this evaluation, refer to Dong & Dong (2021); and Guo *et al.* (2021). The latest CMIP6 combines RCPs and shared socioeconomic pathways (SSPs) to produce a more reasonable future scenario (Peng & Li 2021; Su *et al.* 2021). Four combinations of SSP-RCP scenarios are adopted in this study, which are SSP1-2.6 (sustainability), SSP2-4.5 (middle of the road), SSP3-7.0 (regional rivalry), SSP5-8.5 (fossil fuel development) (Su *et al.* 2021). ‘Nominal Resolution’ is 100 and 250 km. ‘Variant Label’ is r1i1p1f1. They describe possible future worlds and represent different combinations of mitigation and adaptation challenges. SSP1-2.6 has significant changes for land use, and cover ratio of its global forest will increase. The land use and aerosol pathways of SSP2-4.5 are not extreme relative to other SSPs. It combines intermediate societal vulnerability with an intermediate forcing level. SSP3-7.0 is a scenario with a large number of land use changes (especially decreased global forest cover) and high NTCF emissions (especially SO₂).

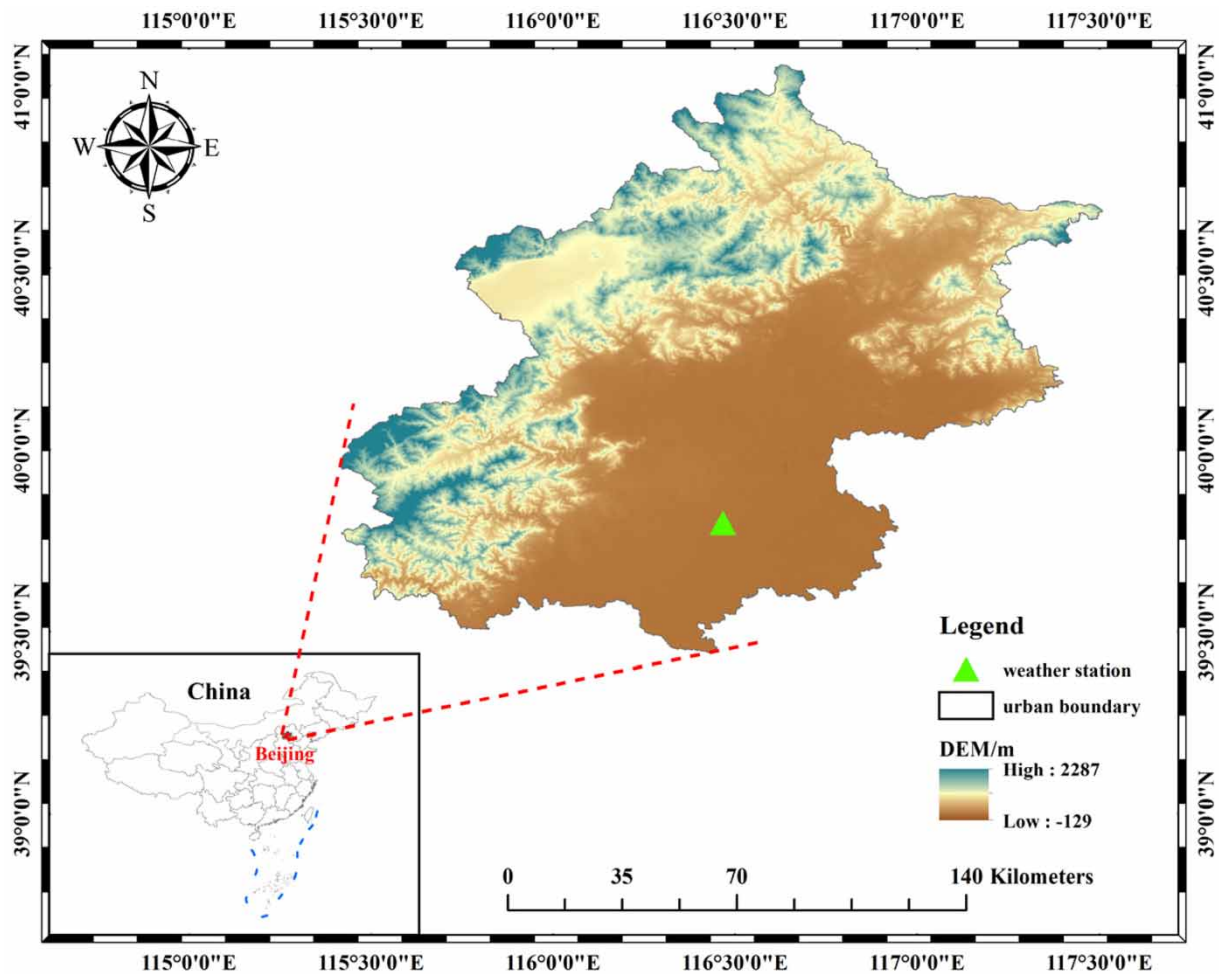


Figure 1 | Distribution map of study area.

Table 1 | List of the CMIP6 GCMs used in this study

No	Model	Institution	Country	Resolution
1	CESM2-WACCM	US National Center for Atmospheric Research (NCAR)	USA	288 × 192
2	CMCC-CM2-SR5	Euro-Mediterranean Center on Climate Change (CMCC)	Italy	288 × 192
3	CMCC-ESM2		Italy	288 × 192
4	MPI-ESM1-2-HR	Max Planck Institute for Meteorology (MPI-M)	Germany	288 × 192
5	MRI-ESM2-0	Meteorological Research Institute (MRI)	Japan	320 × 160
6	NorESM2-MM	NorESM Climate modeling Consortium consisting of CICERO (NCC)	Norway	288 × 192
7	FGOALS-g3	Chinese Academy of Sciences (CAS), China	China	180 × 90
8	TaiESM1	Research Center for Environmental Changes (AS-RCEC)	China	288 × 192
9	ACCESS-CM2	Commonwealth Scientific and Industrial Research Organisation (CSIRO)	Australia	192 × 144
10	ACCESS-ESM1-5			192 × 145
11	CanESM5	Canadian Centre for Climate Modelling and Analysis (CCCma)	Canada	128 × 64
12	MIROC6	Japan Agency for Marine-Earth Science and Technology, Atmosphere and Ocean Research Institute, National Institute for Environmental Studies, and RIKEN Center for Computational Science (MIROC)	Japan	256 × 128

SSP3-7.0 is a scenario with both substantial land use change. SSP5-8.5 is the only SSP scenario with emissions high enough to produce a radiative forcing of 8.5 Wm^{-2} in 2100.

3. RESEARCH METHODOLOGY

3.1. Research framework

The research framework of the study is illustrated in Figure 2. The basic data is preprocessed, which contains: (1) Interpolation of minute-level precipitation and synthesis of precipitation with different durations; (2) Download and extraction of CMIP6 and interpolation of daily data for models with calendar 'noleap'. The frequency distribution parameters of precipitation for the observed sub-daily and the CMIP6 daily are calculated. Previous studies usually choose GEV or Gumbel for fitting of frequency distribution, and this method cannot guarantee that the effect of fitting for discrete frequency points is optimal. Four distribution functions (GEV, Gumbel, Pearson3, and Exponential) were adopted in this study to obtain the best fitting frequency distribution curve. For the historical IDF curve, it is necessary to consider whether there is an extra large value and deal with it before fitting. The existence of this extra large value will increase the rainfall in the high

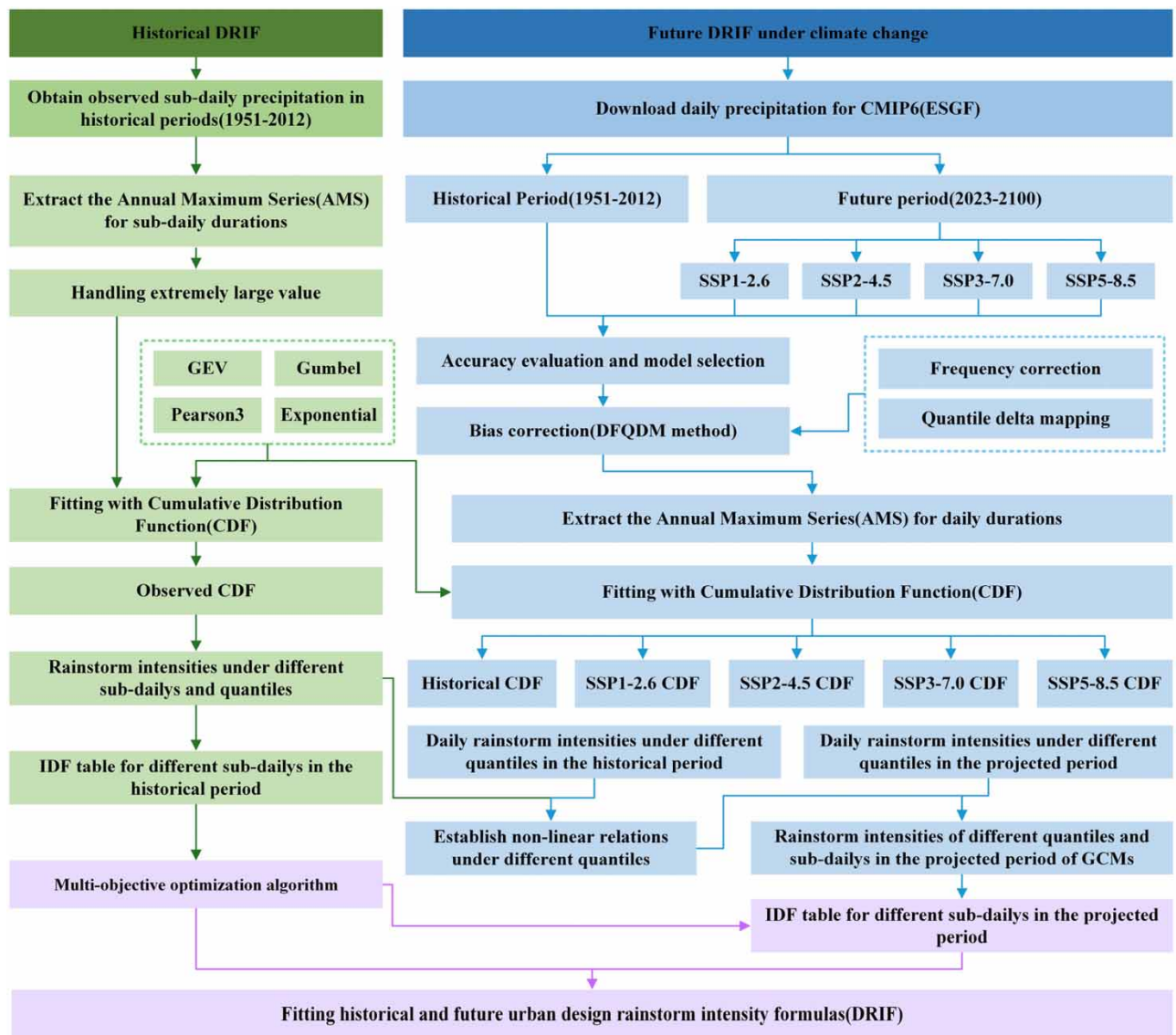


Figure 2 | Research framework of the study.

return period and the design cost of engineering facilities. When the extra large value is processed, the non-linear relationship between the observation and the model is established between the quantiles of different return periods in the historical period. The non-linear contains the functional relationship between the modeled daily and the observed sub-daily curve. This function is applied to the future quantile values of the model. Rainstorm intensity of the model are calculated for different sub-daily and return period in the future. The future IDF curve is established. Finally, the historical and future DRIFs are obtained by fitting the IDF curve using a multi-objective optimization algorithm.

3.2. Outlier detection in extreme value series

Outliers are extreme values that stand out from the distribution of the data in the graph or table. Outliers in the series will affect the statistical results of samples, such as mean, standard deviation, coefficient of variation, skewness coefficient and kurtosis coefficient, thus affecting the parameters of the distribution function. Seven detection methods of outliers were adopted in this study, which are Z-Score (ZS), 3-sigma (3σ), Modified Z-Score (MZS), median absolute deviation (MADe), Box-Plot Method (BPM), Grubbs-Beck Test (GBT), Stedinger Test (ST) (Grubbs 1969; Crosby 1994; Kannan *et al.* 2015; Asikoglu 2017; Lu *et al.* 2018).

- (1) The Z-score assumes that sample x follows normal distribution, which is $X_i \sim N(\mu, \sigma^2)$. The Z-score is calculated as follows:

$$Z_i = \frac{x_i - \bar{x}}{s} \quad (1)$$

where x_i is the sample X ; \bar{x} is mean of sample X ; s variance of sample X . When $Z_i > \gamma$, x_i is the outlier. For the γ , the thresholds used in Asikoglu (2017) and Kannan *et al.* (2015) are 2.5 and 3, respectively. The γ can be adjusted according to the distribution range of abnormal values of sample data, which is 2.5 in this study. The Z-score is greatly affected by outliers and is not suitable for the detection of outliers in small samples.

- (2) The 3-sigma is also known as the 68-95-99.7 rule. It is similar to the calculation principle of the Z-Score. When the γ of the Z-Score is equal to 3, it is the 3-sigma. It assumes that the sample follows a normal distribution, and when the positive or negative moments of the sample data are outside σ , 2σ or 3σ , the data is considered to be an outlier (Figure 3). The

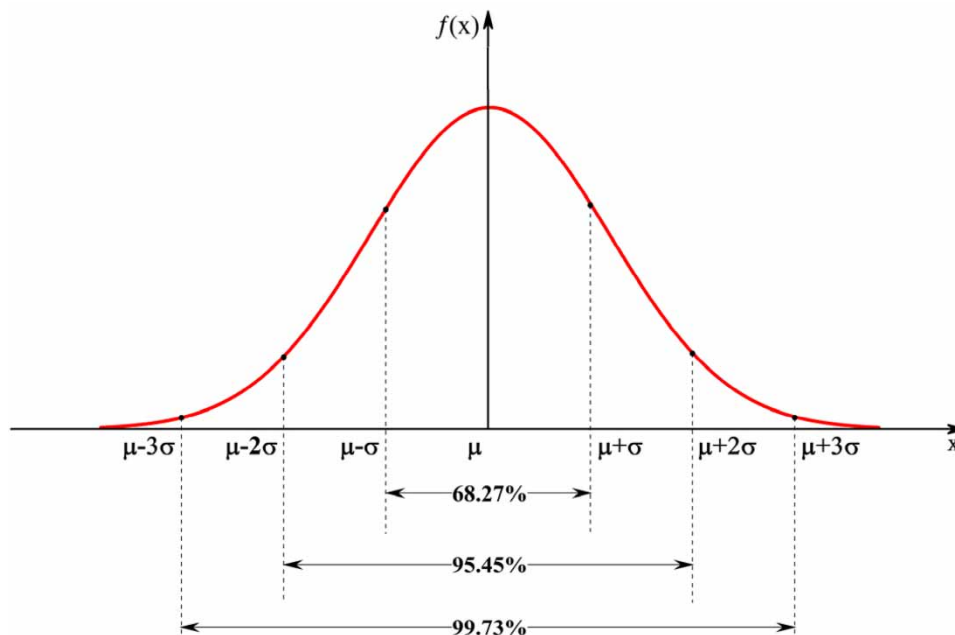


Figure 3 | Distribution diagram of confidence intervals for a normal distribution with 3-sigma rule.

probabilities of x falling within different confidence intervals are as follows:

$$P(\mu - 1\sigma \leq x \leq \mu + 1\sigma) \approx 0.682689492137086 \quad (2)$$

$$P(\mu - 2\sigma \leq x \leq \mu + 2\sigma) \approx 0.954499736103642 \quad (3)$$

$$P(\mu - 3\sigma \leq x \leq \mu + 3\sigma) \approx 0.997300203936740 \quad (4)$$

- (3) The modified Z-score adopts median and median absolute deviation instead of mean and standard deviation, which solves the problem of poor detection ability of Z-score for outliers in small sample data (Kannan *et al.* 2015). When $|z_i| > 3.5$, there are outliers in the sample data. The formula is as follows:

$$z_i = 0.675(x_i - x_{0.5})/MAD \quad (5)$$

$$MAD = \text{median}(|x_i - \text{median}(x)|) \quad (6)$$

where x_i is the sample X; N is the number of data.

- (4) MADe is a stable detection method that is less affected by extreme values. The study adopts the 3MADe method, as follows:

$$2MADe: x_{outlier} \in (-\infty, \text{Median} - 2S) \cup (\text{Median} + 2S, +\infty) \quad (7)$$

$$3MADe: x_{outlier} \in (-\infty, \text{Median} - 3S) \cup (\text{Median} + 3S, +\infty) \quad (8)$$

$$S = 1.4826 \times \text{median } |x_i - \text{median}(x)| \quad (9)$$

where $x_{outlier}$ is the outlier; x_i is the sample X.

- (5) The boxplot obtains the interquartile range IQR by calculating the difference between the upper quartile Q_3 and the lower quartile Q_1 of the sample, and which is suitable for dealing with symmetric and skewed data. In the study, IQR15 is adopted as the judgment criterion for outliers (Saleem *et al.* 2021):

$$IQR = Q_3 - Q_1 \quad (10)$$

$$IQR15 \in (-\infty, Q_1 - 1.5IQR) \cup (Q_3 + 1.5IQR, +\infty) \quad (11)$$

$$IQRM \in (Q_1 - 3IQR, Q_1 - 1.5IQR) \cup (Q_3 + 1.5IQR, Q_3 + 3IQR) \quad (12)$$

$$IQR30 \in (-\infty, Q_1 - 3IQR) \cup (Q_3 + 3IQR, +\infty) \quad (13)$$

where IQR is interquartile range; $IQR15$ is the outlier; $IQRM$ is potential or moderate outliers; $IQR30$ is extreme outliers.

- (6) The Grubbs-Beck Test defines a set of high and low thresholds X_H and X_L . When the sample x is greater than X_H , it is a high outlier, or when the sample x is less than X_L , it is a low outlier:

$$X_H = \bar{x} + k_N \cdot S_x \quad (14)$$

$$X_L = \bar{x} - k_N \cdot S_x \quad (15)$$

where \bar{x} is mean of sample X; k_N is the threshold at different significance levels, this study adopts the 0.01 significance level. Its value can refer to Grubbs & Beck (1972); S_x is standard deviation.

- (7) Stedinger Test defines a set of high and low thresholds X_H and X_L . When the sample x is greater than X_H , it is a high outlier, or when the sample x is less than X_L , it is a low outlier:

$$y_i = \ln x_i \quad (16)$$

$$X_H = \exp(\bar{y} + k_N \cdot S_y) \quad (17)$$

$$X_L = \exp(\bar{y} - k_N \cdot S_y) \quad (18)$$

$$k_N = -0.9043 + 3.345\sqrt{\log N} - 0.4046 \log N \quad (19)$$

where x_i is sample X ; \bar{y} is mean of y_i ; S_y is standard deviation of y_i ; k_N is the threshold.

3.3. Processing of extreme value

For extreme values, this study focuses on outliers that have a greater effect on the higher return period of the frequency curve. When the series of the sample is judged to have an extreme value, the extra-large value will be processed in three ways: (1) Extracting the second maximum value of the daily precipitation in the i th year(SMV); (2) Extract the average value of the daily precipitation in the i th year that is greater than the critical value(AVG); (3) Extracting the maximum value of the daily precipitation in the i th year which is less than the critical value (MVL). First, the maximum daily precipitation for each year is extracted to form a statistical sample. When it is judged that there is an extreme value in this sample, the data of the year in which the extreme value is located will be processed. The data of this year are sorted in descending order, and the second largest value is extracted and used to replace the i th extreme value in the sample. This processing method is the principle of SMV. The calculation methods of AVG and MVL are similar to SMV. They extract respectively the average value of daily data greater than the critical value and the maximum value of daily data less than the critical value in the year where the extreme value is located.

3.4. Calculation of IDF curve under climate change

Step 1: The climate model was corrected using a quantile delta mapping method of daily precipitation based on frequency (DFQDM). The method can correct the frequency and value of wet days of precipitation. This 95th percentile was used to divide monthly precipitation into normal and extreme precipitation. A mixed Gamma distribution was used to fit the cumulative distribution frequency(CDF) of the two parts of the daily precipitation. A quantile delta map was used to correct for precipitation.

Step 2: $x_{ij,max}^{OBS}$ is the maximum value of the extracted observations in the j th duration of the i th year. The number of durations of the precipitation in this study contains 15, which are 5, 10, 15, 20, 30, 45, 60, 90, 120, 150, 180, 240, 360, 720 and 1440. This duration takes into account both short and long-duration precipitation. The simulation of urban drainage system is more concerned with the simulation of short-duration precipitation process.

Step 3: $x_{i,daily,max}^{GCM,REF}$ and $x_{i,daily,max}^{GCM,FUT}$ are the maximum daily precipitation (1440 min) of the i th year in the historical and future periods of the extracted model, respectively;

Step 4: Frequency distributions of observation and model are fitted:

$$Prob(OBS) = f(\theta^{OBS,subdaily}, x_{subdaily,max}^{OBS}) \quad (20)$$

$$Prob(GCM_{REF}) = f(\theta^{REF,daily}, x_{daily,max}^{REF}) \quad (21)$$

$$Prob(GCM_{FUT}) = f(\theta^{FUT,daily}, x_{daily,max}^{FUT}) \quad (22)$$

Step 5: The rainstorm intensity under different quantiles or return periods is calculated. The return period ranges from 2- to 100-years, and the interval is taken as 0.5-year:

$$Y_{RP}^{OBS,subdaily} = F^{-1}\left(\left(1 - \frac{1}{RP}\right) | \theta^{OBS,subdaily}\right) \quad (23)$$

$$Y_{RP}^{REF,daily} = F^{-1}\left(\left(1 - \frac{1}{RP}\right) | \theta^{REF,daily}\right) \quad (24)$$

$$Y_{RP}^{FUT,daily} = F^{-1}\left(\left(1 - \frac{1}{RP}\right) | \theta^{FUT,daily}\right) \quad (25)$$

Step 6: A non-linear relationship between the quantiles of observed sub-daily and modeled daily is established over the historical period. The purpose is to obtain a quantitative relationship between the CDF curves of observation and model under different return periods:

$$Y_{RP}^{OBS,subdaily} = A \times Y_{RP}^{REF,daily} + b \quad (26)$$

Step 7: It is assumed that the non-linear relationship applies to the future period of model. The rainstorm intensities of sub-daily under different return periods for the future period are calculated. The result can be extracted to obtain the IDF table or fitted to obtain the DRIF:

$$Y_{RP}^{FUT,subdaily} = A \times Y_{RP}^{FUT,daily} + b \quad (27)$$

3.5. Design rainstorm intensity formula (DRIF)

The frequency distribution curve for different return periods and durations has a large number of parameters. It is very inconvenient for the designer to apply it. A common practice is to adopt DRIF to fit the IDF table. The form of DRIF adopted in China are as follows:

$$q = \frac{A_1(1 + C \times \lg P)}{(t + b)^n} \quad (28)$$

where A_1 , b and c are the parameters to be solved; q is rainstorm intensity, mm/min; t is the duration, min; If the unit of q is converted to $[L/(hm^2 \cdot s)]$, the right side of the above equation will be multiplied by 167.

3.6. Frequency distribution and multi-objective optimization algorithms

GEV, Gumbel, Pearson3, Exponential are adopted to compare and obtain the best distribution function of empirical frequency points in this study. In the process of parameter optimization of the frequency distribution curve and DRIF, this study adopts several widely used solution methods. They are respectively L-moment (Kotz & Nadarajah 2000), Multistart search least squares algorithm (MSLSA) (Ugray *et al.* 2007), Non-dominated sorting genetic algorithm II (NSGAI) (Deb *et al.* 2002), Multi-objective particle swarm optimization (MOPSO) (Coello & Lechuga 2002), Multi-objective evolutionary algorithm based on decomposition (MOEA/D) (Zhang & Li 2007), Nondominated sorting and local search (NSLS) (Chen *et al.* 2014). The formula for the error of the fitting accuracy for DRIF is as follows:

(1) Mean absolute root mean square error (MARMSE):

$$X_m = \sqrt{\frac{1}{n} \sum_{i=1}^n (q' - q)^2} \quad (29)$$

(2) Mean relative root mean square error (MRRMSE):

$$U_m = \sqrt{\frac{1}{n} \sum_{i=1}^n \left(\frac{q' - q}{q} \right)^2} \times 100\% \quad (30)$$

where q' is rainstorm intensity fitted to theoretical frequency curve (X_m) or DRIF (U_m), mm/min; q is the rainstorm intensity fitted by empirical frequency curve (X_m) or theoretical frequency curve (U_m), mm/min; n is the number of sample data.

The selection of the distribution function is based on the performance of MARMSE and MRRMSE for the DRIF. In China, the regulations promulgated by the Ministry of Housing and Urban-Rural Development (MOHURD) require that when the return period is two to 20 years, MARMSE should not be greater than 0.05 mm/min in areas with general rainstorm intensity, and MRRMSE should not be greater than 5% in areas with large rainstorm intensity. The accuracy of this calculation was evaluated using two- to 100-years when the DRIF was fitted. The interval of this return period is taken as 0.5 years. The accuracy requirements for MRRMSE and MARMSE are for DRIF rather than IDF in this study. These two indicators can be used as an evaluation index for the accuracy of the fitting of the IDF curve.

4. RESULTS

4.1. Changes in annual precipitation for historical and future periods

The annual precipitation of SSP3-7.0 is the maximum in many years (Figure 4). In the historical period, the annual average precipitation of the observation and the model is 592.8 and 590.6 mm, respectively. The annual mean precipitation of the corrected model is very close to the observation. The annual average precipitation of the model in the future period is 765.2, 793.4, 848.9, and 927.9 mm, respectively. With the increase of radiation, the annual average precipitation is gradually increasing. The order of the magnitude is SSP1-2.6 < SSP2-4.5 < SSP3-7.0 < SSP5-8.5. Under the four scenarios, the variation of the model relative to the observation was 29.09, 33.84, 43.21 and 56.52%, respectively. The maximum values of precipitation of observation and model are 1406 and 1336 mm in the historical period. The maximum precipitation of the model is respectively 1506.9, 1628.9, 1661.3 and 1981.8 mm in the future period. The maximum annual precipitation of the observation occurred in the year 1959, which was 1406 mm. The precipitation in the future period showed a significant increase trend, and the rates of change were 1.6, 3.3, 2.6 and 6.3 mm/year, respectively.

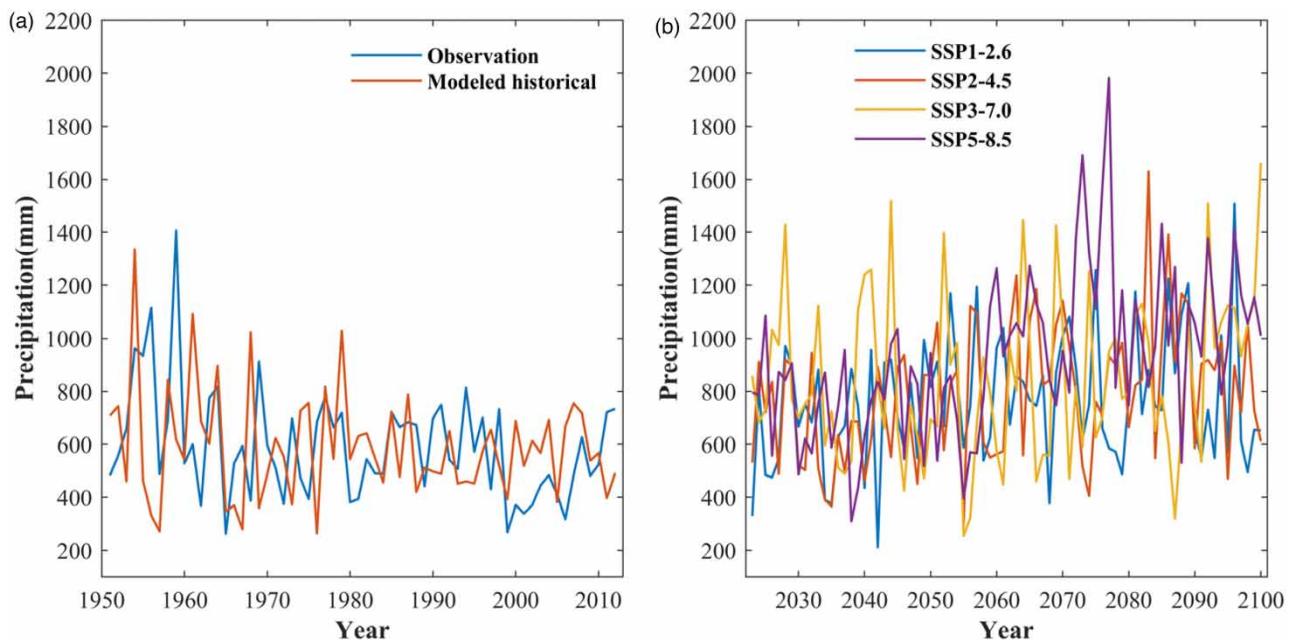


Figure 4 | Change of annual precipitation for model and observation.

4.2. Calculation of DRIF for historical periods

It can be seen from Table 2 that the solution method and frequency distribution of DRIF to meet the requirements of the fitting accuracy are the Exponential optimized by NSGA-II, the Gumbel optimized by MOEA/D, and the Gumbel distribution optimized by NSLS. The optimized accuracy of NSLS is better than that of NSGA-II, NSGA-III and MOEA/D, and the Gumbel has the best performance. The MARMSE and MRRMSE of NSLS were 0.045 and 3.475%, respectively. The MRRMSE is the lowest among all distributions. The coefficient of determination (R^2) is close to 1. In this 100-year return period and different durations, the intensity of the rainstorm varies from 0.169 to 4.124 mm/min. The MARMSE and MRRMSE of the L-moment do not meet the accuracy requirements. L-moment was established by Hosking in 1990 and is widely used in fields such as hydrology and civil engineering (Wan Zin *et al.* 2009). Compared with other methods of moments, the main advantage of the L-moment method is that it is less affected by the variability of the samples (Břlková 2012). The L moment is more stable and the solution speed is faster, and it can provide safer results in the case of small samples. When the IDF table needs to be obtained quickly, the L-moment method is an optimal choice. MOPSO has the advantages of easy implementation and fast search. The main disadvantage of this algorithm is that the non-dominated solutions of uniform distribution in the solution space are poorer and the diversity of solutions is insufficient (Zhang *et al.* 2016). NSGA-II and MOEA/D are the most widely used multi-objective optimization algorithms. The disadvantage of NSGA-II is that it performs poorly on high-dimensional problems when the number of objective functions exceeds three (Zhao & Li 2014; Huang *et al.* 2019). The probability of crossover and mutation of NSGA-II is not perfect, and its process of calculation is very time-consuming. MOEA/D has problems such as reduced population evolution efficiency and poor evolution quality in the calculation process. It may be due to the above shortcomings that the performance of these algorithms is not as well as that of NSLS. NSLS is able to find better distributions of solutions and better convergence to true pareto optimal frontiers (Chen *et al.* 2014). The Gumbel optimized for the NSLS will be adopted to compute the historical DRIF in this study.

Table 2 | Results of parameter optimization and accuracy evaluation for DRIF in historical periods

Optimization method	Type of frequency distribution	R^2	MARMSE	MRRMSE (%)	A1	C	b	n
L-moment	Pearson3	0.997	0.060	5.489	16.834	0.993	22.036	0.768
	Gumbel	0.999	0.028	7.494	12.379	0.801	14.732	0.704
	GEV	0.995	0.077	5.524	14.916	1.419	23.958	0.782
	Exponential	0.999	0.033	7.988	9.591	1.373	15.047	0.699
MSLSA	Pearson3	0.997	0.067	5.097	17.580	1.424	26.131	0.800
	Gumbel	0.999	0.035	7.043	13.227	0.897	16.422	0.716
	GEV	0.994	0.092	5.660	12.427	3.317	31.603	0.840
	Exponential	0.999	0.044	6.783	11.175	1.466	18.175	0.726
NSGA-II	Pearson3	0.996	0.068	4.983	18.572	1.411	26.979	0.809
	Gumbel	0.999	0.036	6.206	13.562	0.923	16.897	0.725
	GEV	0.994	0.092	5.867	11.454	3.329	30.337	0.826
	Exponential	0.998	0.049	3.909	14.419	1.521	21.900	0.781
MOPSO	Pearson3	0.994	0.086	15.924	38.189	1.278	36.406	0.931
	Gumbel	0.986	0.127	8.850	8.020	3.991	25.825	0.834
	GEV	0.992	0.110	6.712	2.486	20.776	32.658	0.858
	Exponential	0.995	0.081	10.794	41.307	1.198	34.180	0.949
MOEA/D	Pearson3	0.997	0.064	4.519	23.098	1.435	29.792	0.855
	Gumbel	0.998	0.045	3.876	20.595	0.924	22.230	0.807
	GEV	0.995	0.088	5.247	11.680	3.637	31.456	0.845
	Exponential	0.998	0.051	3.755	15.762	1.564	23.558	0.801
NSLS	Pearson3	0.997	0.068	4.496	19.380	1.516	28.121	0.827
	Gumbel	0.998	0.045	3.475	15.335	1.107	19.922	0.771
	GEV	0.994	0.092	5.713	11.086	3.489	30.400	0.828
	Exponential	0.997	0.059	7.625	7.015	2.250	15.877	0.701

The IDF curve optimized by the NSLS is shown in Figure 5. The error of the fitting for Gumbel is larger at higher return periods. The same effect occurs with the Pearson3. The fitting effect of GEV and Exponential is better for the tail of the IDF curve. However, these two distribution functions are too close to the rainstorm intensity for the return period of more than 60-years, which leads to poor fitting accuracy for the low return period. The 10 and 20-min curves of the GEV may intersect after the 100-year return period. This would result in the same rainstorm intensity for different durations in a certain return period, which is unreasonable. At the same time, the rainstorm intensity for the high return period will increase significantly compared with the low return period. This phenomenon indicates that there may be an extreme value in this series. Affected by extreme values, IDF has a better effect on the simulation of low return periods and is poorer for high return periods. The design of urban drainage system pays more attention to short duration and low return period precipitation. The precipitation for this return period in the range of two-year to 20-years is important. In order for the IDF curve to take into account the accuracy of the simulation for both high and low return periods, the extreme values of the sample should be treated as more reasonable ranges.

4.3. Calculation of DRIF considering the influence of extra-large value on IDF

Figure 6 shows the size and number of the critical value for different judgment methods of extreme value. Since the critical values of Z-Score and Modified Z-Score are constant, they first transform on the original data and then compare the size with the critical value. Therefore, their critical values do not change with different durations in the figure. This study only compares the magnitude of the critical value for other methods. Critical value of Stedinger is the largest. The critical values for MADE and Boxplot are minimal since the values of the samples are all smaller than the critical value of Stedinger.

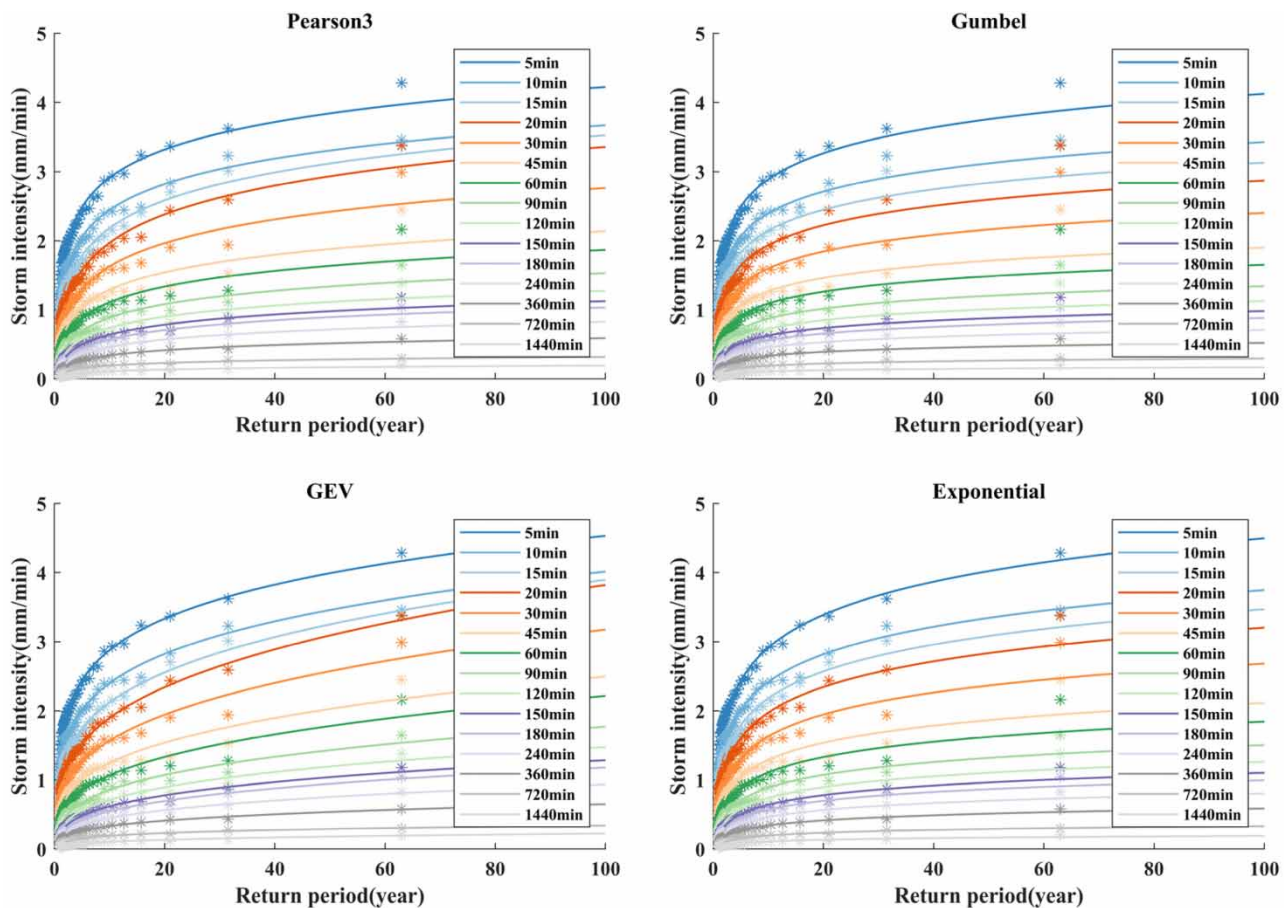


Figure 5 | IDF curve optimized by NSLS without outlier handling.

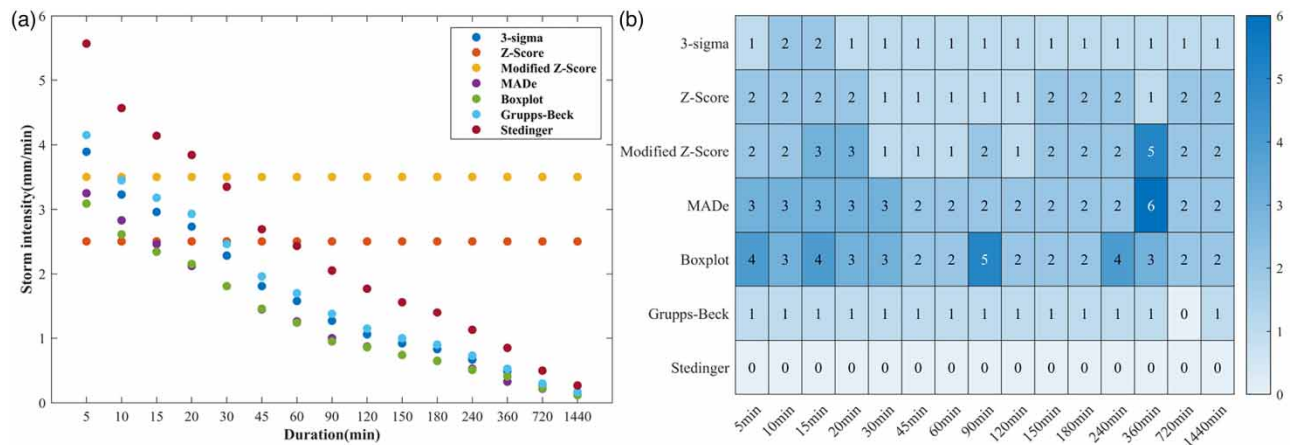


Figure 6 | Critical values for different outlier judgment methods: (a) The size; (b) The number.

The number of extreme values detected by Stedinger is 0. The number of extreme values judged by MaDe at the 360 is the largest, which is 6.

Table 3 indicates that the accuracy of the DRIF is optimized by the NSLS after the outliers are processed. There are many judgment methods for outlier processing that meet the accuracy requirements of the fitting. The comprehensive rating index (CRI) was adopted in this study to select the best outlier handling method for the fitting (Zhang *et al.* 2018). The CRI can calculate a comprehensive index by ranking the different evaluation indicators. In this study, R^2 , MARMSE and MRRMSE were selected to calculate the CRI. It can be seen from Table 3 that the Boxplot of SMV, the Z-Score of AVG and the Z-Score of MVL have the highest CRI, which are all 0.583. From the optimization results of this IDF curve, it can be seen that the error of SMV in the high return period is still larger (Figure 7). The reason is that when extracting the second value of the year in which the outlier is located, the second rainstorm intensity is very close to the first one. Therefore, the distribution of this empirical frequency point has not changed much. The accuracy of the fitting for AVG is better and the

Table 3 | Accuracy of fitting after outliers are processed

Handling Method	Judgment method	R^2	MARMSE	MRRMSE(%)	CRI
SMV	3-sigma	0.9980	0.0482	4.2961	0.208
	Z-Score	0.9990	0.0345	6.8189	—
	Modified Z-Score	0.9989	0.0348	6.0390	—
	MADe	0.9990	0.0341	6.9258	—
	Boxplot	0.9989	0.0345	4.9678	0.583
	Gruppss-Beck	0.9987	0.0381	4.5642	0.542
	Stedinger	0.9989	0.0356	6.9546	—
AVG	3-sigma	0.9990	0.0332	5.5602	—
	Z-Score	0.9985	0.0402	3.9388	0.583
	Modified Z-Score	0.9991	0.0320	7.4550	—
	MADe	0.9992	0.0294	8.5145	—
	Boxplot	0.9963	0.0629	6.3776	—
	Gruppss-Beck	0.9986	0.0407	4.1338	0.542
	Stedinger	0.9989	0.0356	6.8886	—
MVL	3-sigma	0.9982	0.0445	4.6060	0.208
	Z-Score	0.9986	0.0377	4.2271	0.583
	Modified Z-Score	0.9977	0.0490	4.1278	0.250
	MADe	0.9993	0.0268	8.0646	—
	Boxplot	0.9949	0.0692	6.9804	—
	Gruppss-Beck	0.9992	0.0308	6.2984	—
	Stedinger	0.9989	0.0360	5.8671	—

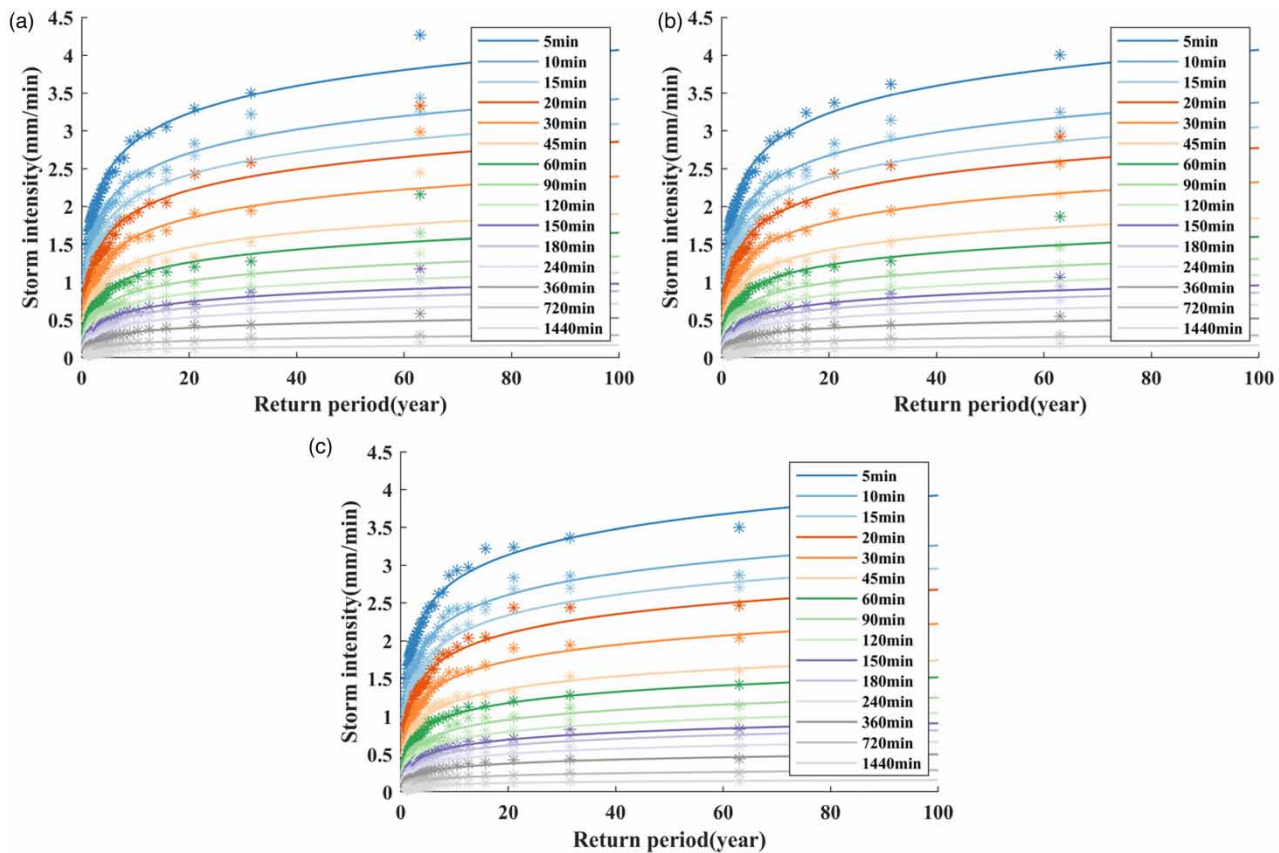


Figure 7 | Optimization results of IDF curves after outlier processing. (a) SMV; (b) AVG; (c) MVL.

distribution of the empirical frequency point is better. The rainstorm intensity of MVL in the high return period is obviously reduced, and the rainstorm intensity greater than the 30-year return period is very close. When the maximum value is less than the critical value, it will seriously underestimate the rainstorm intensity in this high return period. Z-score and AVGs are recommended for the judgment and treatment of outliers in the study.

4.4. Comparison of IDF values before and after processing of extra large values

After the outliers are processed, the rainstorm intensity is slightly reduced in different return periods compared with before processing. In Table 4, the color of dark red represents a larger proportion of reduction, and the color of dark green represents a smaller proportion of reduction. The proportion of this reduction increases as the return period increases. The scale of this reduction varies from -0.1 to -3.1% , with a slight decrease in value. The Z-score method did not change the value of the sample points significantly, and the ratio was the largest at 60-min.

The calculation results of the DRIF for the historical period are as follows:

(1) No handling of outliers

$$q = \frac{15.335(1 + 1.107 \times \lg P)}{(t + 19.922)^{0.771}}$$

(2) Handling of outliers

$$q = \frac{15.618(1 + 0.937 \times \lg P)}{(t + 18.686)^{0.761}}$$

4.5. Calculation of DRIF under climate change

The future scenario is fitted separately by four distribution functions. The optimal combination of the function is shown in Table 5. This combined distribution function is adopted to reflect the change of the real frequency point as much as possible, which is different from other studies. For example, both Butcher & Zi (2019) and Tousi *et al.* (2021) adopted the GEV when

Table 4 | The percentage of change in rainstorm intensity before and after outlier processing

Return period(year)	Duration(min)														
	5	10	15	20	30	45	60	90	120	150	180	240	360	720	1440
2	-0.1%	-0.2%	-0.3%	-0.3%	-0.4%	-0.3%	-0.4%	-0.3%	-0.3%	-0.4%	-0.4%	-0.2%	-0.2%	-0.1%	-0.3%
3	-0.4%	-0.5%	-0.9%	-1.1%	-1.1%	-1.0%	-1.2%	-0.9%	-1.0%	-1.0%	-1.0%	-0.7%	-0.5%	-0.4%	-0.7%
5	-0.6%	-0.8%	-1.4%	-1.7%	-1.7%	-1.6%	-1.8%	-1.4%	-1.5%	-1.5%	-1.5%	-1.1%	-0.7%	-0.5%	-1.1%
10	-0.8%	-1.1%	-1.8%	-2.3%	-2.3%	-2.1%	-2.4%	-1.8%	-1.9%	-1.8%	-1.9%	-1.4%	-0.9%	-0.7%	-1.3%
20	-1.0%	-1.2%	-2.2%	-2.7%	-2.6%	-2.4%	-2.8%	-2.1%	-2.2%	-2.1%	-2.2%	-1.6%	-1.0%	-0.8%	-1.5%
30	-1.1%	-1.3%	-2.3%	-2.9%	-2.8%	-2.6%	-2.9%	-2.2%	-2.4%	-2.2%	-2.3%	-1.7%	-1.1%	-0.8%	-1.6%
50	-1.1%	-1.4%	-2.5%	-3.1%	-3.0%	-2.7%	-3.1%	-2.3%	-2.5%	-2.4%	-2.4%	-1.8%	-1.1%	-0.8%	-1.7%
100	-1.2%	-1.6%	-2.7%	-3.3%	-3.2%	-2.9%	-3.3%	-2.5%	-2.7%	-2.5%	-2.6%	-1.9%	-1.2%	-0.9%	-1.8%

Table 5 | Fitting results of frequency distribution of different scenarios in the future

Model	Frequency distribution	R ²	MARMSE	MRRMSE (%)
Ref	Pearson3	0.98	0.003	4.801
SSP1-2.6	GEV	1.00	0.002	6.083
SSP2-4.5	GEV	0.97	0.006	7.642
SSP3-7.0	GEV	0.99	0.003	4.211
SSP5-8.5	Pearson3	0.98	0.004	5.920

fitting the CDFs of observation and model. [Srivastav et al. \(2014\)](#) adopted the Gumbel. For all scenarios, a single distribution may not be optimal for reflecting the change of CDF. It can be seen from [Figure 8](#) that the performance of this fitting is very good. The fitting of the frequency curve of the observation has not been processed by outliers. MARMSE and MRRMSE in [Table 5](#) are both small.

[Figure 9](#) shows that the fitting results of the rainstorm intensity of the quantile under different durations of observation and model in the historical period. There is a perfect non-linear relationship between the rainstorm intensity of the modeled daily and the observed sub-daily. The expression and precision of this fitting are shown in this figure. The R² is close to 1 and the RMSE is close to 0. This expression can quantitatively reflect the relationship of CDF between the model and the observation. The form of this functional relation is the same as that obtained by [Requena et al. \(2021\)](#). This quantitative relationship is assumed to apply for the future period of the model. The IDF table for the future period is calculated. This study adopts 3D surfaces to compare the size of IDF in space ([Figure 10](#)). This duration is divided into four parts: the first part (5-, 10- and 15-min), the second part (20-, 30- and 45-min), the third part (60-, 90-, 120- and 150-min), the fourth part (180-, 240-, 360-, 720- and 1440-min). The order of the size of the SSP is different for different return periods in the future. When the return period is greater than 40 years, SSP2-4.5 > SSP5-8.5 > SSP1-2.6 > SSP3-7.0 > Observation. The design of urban drainage system mostly adopts the process of short-duration precipitation. For duration of the 120-min, SSP5-8.5 > SSP3-7.0 > SSP1-2.6 > SSP2-4.5 > Observation at return periods of two, three, five, and 10 years. At 20- and 30-year return periods, SP5-8.5 > SSP2-4.5 > SSP1-2.6 > SSP3-7.0 > Observation. At 50- and 100-year return periods, SSP2-4.5 > SSP5-8.5 > SSP1-2.6 > SSP3-7.0 > Observation. Models do not have a fixed size order in future scenarios.

The calculation results of DRIF from 2023 to 2100 are as follows:

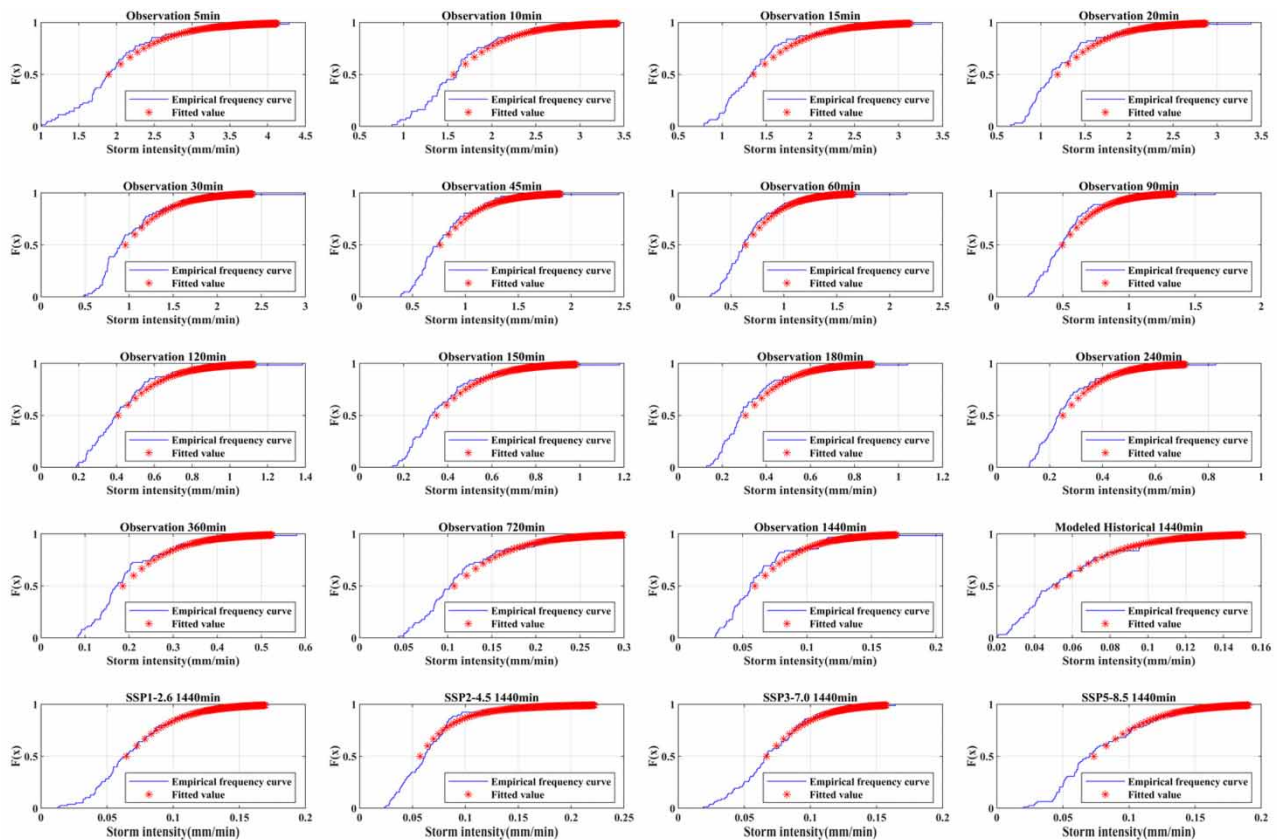


Figure 8 | Fitting results of empirical frequency curves of observation and model for historical and future periods.

$$\text{SSP1-2.6: } q = \frac{17.597(1 + 0.925 \times \lg P)}{(t + 19.494)^{0.75}}$$

$$\text{SSP3-7.0: } q = \frac{22.705(1 + 0.638 \times \lg P)}{(t + 20.357)^{0.772}}$$

$$\text{SSP2-4.5: } q = \frac{7.500(1 + 4.287 \times \lg P)}{(t + 22.388)^{0.776}}$$

$$\text{SSP5-8.5: } q = \frac{24.647(1 + 0.744 \times \lg P)}{(t + 21.374)^{0.768}}$$

Optimization results of parameters of DRIF from 2023 to 2100 are shown in Table 6.

4.6. Changes in equivalent return periods for historical and future periods

Figure 11 indicates that the change in the observation for the historical period relative to the equivalent return period of the four scenarios (SSP1, SSP2, SSP3, SSP5) for the modeled projected period. The return period under the future scenario corresponding to the return period of this historical period of two, three, five, 10, 20, 30, 50, 100 years is calculated. The change of equivalent return period for 60-, 120-, 180- and 1440-min is shown in Figure 11. Except for SSP2-4.5, the return period of the observations in the historical period is larger than the equivalent return period under other SSP scenarios. Equivalent return periods at two and three years for SSP2-4.5 are slightly larger than observations. For the 100-year return period, the equivalent return period of the observation is all less than the 70-year in the future period. The equivalent return period of SSP1-2.6, SSP2-4.5 and SSP5-8.5 of the 100-year for the observation is less than 40-, 30- and 20-year, respectively. The 100-year equivalent return period under SSP3-7.0 is larger than other future scenarios, which are all less than 70 years. The results show that the design return period of urban drainage facilities will gradually decrease in the future period. The design return period of the built project can no longer meet the requirements of future waterlogging prevention. For SSP2-4.5, the equivalent return period of two- and three is very close to the historical period. For the short-duration precipitation of 120-min, the 100-year equivalent return periods under the four scenarios are 35-, 20-, 54- and 17-year, respectively. This analysis shows that the current infrastructure is only able to resist rainstorm with a 30-year return period under the future

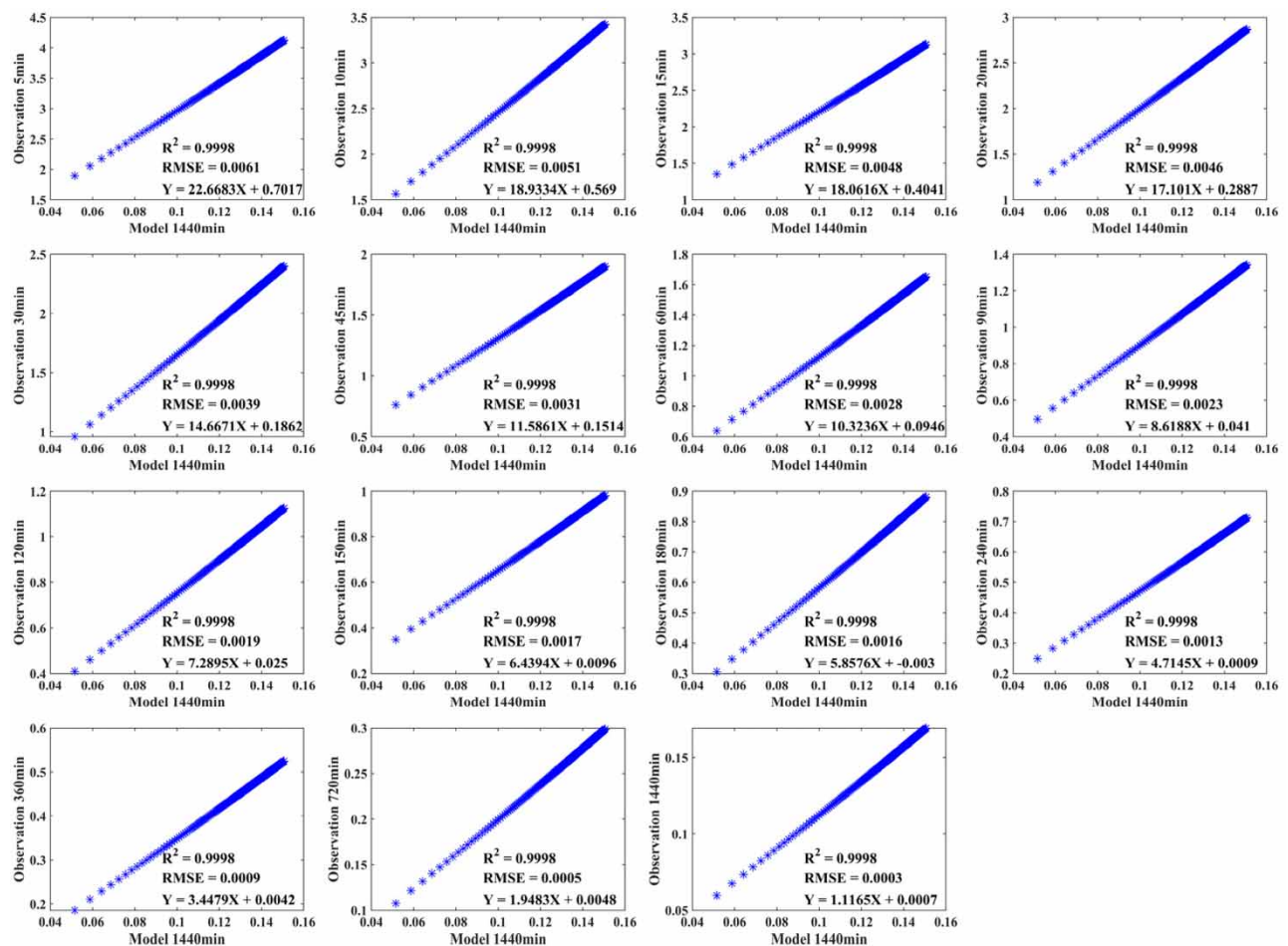


Figure 9 | Results of non-linear fitting of the rainstorm intensity for the quantile of different durations.

SSP1-2.6. Therefore, design of the infrastructure during the historical period should take into account the increase in the intensity of rainstorms in the future.

5. DISCUSSION

At present, there are few relevant studies on the influence of extreme values on the IDF curve. A variety of judgment methods and replacement schemes for outlier are adopted in this study, and the purpose is to propose a more reasonable method for generating IDF curves. This combined method can prevent IDF curve from overestimating the rainstorm intensity in the high return period. In this study, this method is only compared and verified in a weather station, so it may have some uncertainty and still needs further verification. This study proposes a suitable method for replacement of the extreme value for the IDF. For the solution of IDF curve in the future, the previous research mainly includes four methods: (1) After the climate model is corrected, the frequency distribution of historical and future precipitation is fitted. It is assumed that the ratio of rainstorm intensity on daily and sub-daily of observation under different return periods does not change in the future. The daily IDF of the future period is corrected by the ratio to obtain the IDFs of the sub-daily (Tousi *et al.* 2021); (2) This second method is similar to the first method. Daily frequency curves for model and observation are calculated. The ratio of daily precipitation under different return periods of model for the historical and future period is calculated. This ratio is used to obtain the future IDF by correcting the frequency curve of the observed sub-daily. This method is a simplified processing method (Zhou *et al.* 2018); (3) First, the frequency distribution of historical periods is calculated. Quantile mapping is adopted to establish the non-linear relationship between the rainstorm intensity of modeled daily and the observed sub-daily in the historical period. Estimates of rainstorm intensity for different return periods and durations of the model over the historical

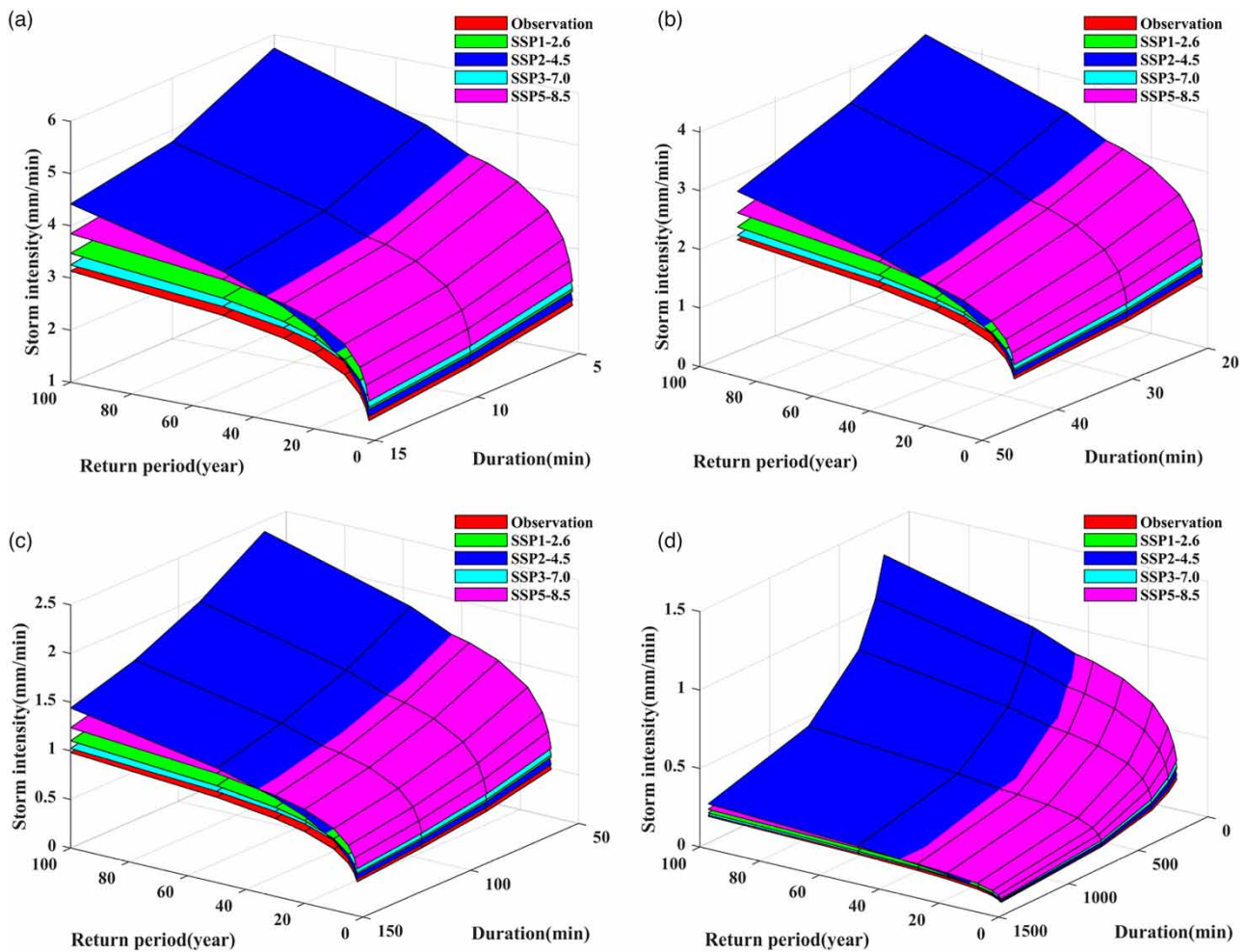


Figure 10 | Surface plots of the IDFs of model under the future different durations and return periods. (a) 5-, 10-, 15-min; (b) 20-, 30-, 45-min; (c) 60-, 90-, 120-, 150-min; (d) 180-, 240-, 360-, 720-, 1440-min.

Table 6 | Optimization results of parameters of DRIF for future period

Scenarios	R^2	MARMSE	MRRMSE(%)	A_1	c	b	n
SSP1-2.6	0.998	0.048	4.351	17.597	0.925	19.494	0.750
SSP2-4.5	0.997	0.080	4.795	7.500	4.287	22.388	0.776
SSP3-7.0	0.998	0.045	3.699	22.705	0.638	20.357	0.772
SSP5-8.5	0.998	0.055	4.104	24.647	0.744	21.374	0.768

period were calculated. Then, adopting the same method as (2), the estimated value of the modeled IDF of in historical period is modified to obtain the IDF of the future period. *Srivastav et al. (2014)* adopts this method to calculate the IDF for the future period. However, this study has many shortcomings. It does not adopt equidistant quantile mapping (EQM). The non-linear relationship of the IDF curve established by this study is the relationship between the modeled future daily and the observed sub-daily. This relationship cannot express the relationship between the IDF of future daily and sub-daily; (4) High-resolution precipitation for this future period is generated based on the random weather generator (*Mirhosseini et al. 2013; Doi & Kim 2021*). The method has great uncertainty for the generation of precipitation. The IDF tables for future periods generated by the models of different weather generators may be different.

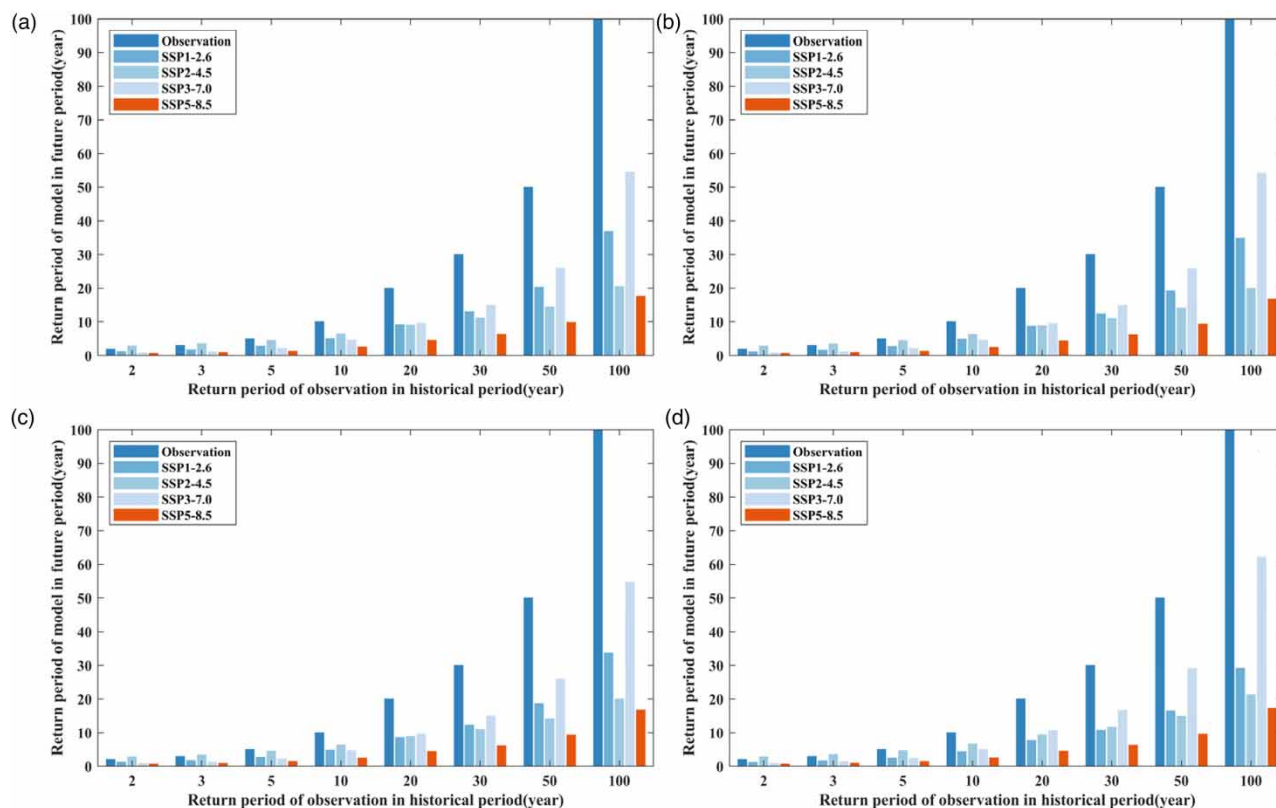


Figure 11 | Change of equivalent return period of observation under climate change. The duration of the precipitation is respectively (a) 60-min; (b) 120-min; (c) 180-min; (d) 1440-min.

The difference between this study and others is that the precipitation of the model is corrected to establish a non-linear relationship between the model and the observation in different sub-dailys of the historical period. The non-linear relationship of the maximum precipitation in different years for the historical period is also applicable in the future period, especially for the near and medium term of the future period. The daily CDF of this future period is calculated using the non-linear relationship established by the historical period to obtain the IDF table of the sub-daily. Therefore, the method established by this study should be more reasonable. In Figure 10, the IDF of different scenarios in this future period are all larger than the observation in the historical period. However, *Tousi et al. (2021)* indicated that the rainstorm intensity of SSP2 of MPI-ESM1-2-HR for the partial return period of 1440-min is smaller than the observation. Therefore, it may be unreliable to directly use the corrected climate model to calculate the IDF table for future periods. The choice of the climate model should first be evaluated for accuracy in the historical period. The model with the best performance of this accuracy can then be used to calculate the IDF table for the future period. The study finally calculates three types of DRIFs, which are respectively: (1) historical periods without outlier processing, (2) historical periods with outlier processing, (3) future periods with different SSP scenarios. The specification of MOHURD does not mention a requirement for the accuracy of the fit of the DRIF for future periods. According to the requirements of the accuracy of this observation, this future DRIF does not meet the conditions. However, the error of the future DRIF calculated by this study is very low, which can meet the design requirements of the infrastructure.

6. CONCLUSION

This research has established an overall framework for calculating DRIF, which includes historical and future periods. This DRIF is obtained based on the fitting of IDF table. Therefore, this research focuses on the generation of the IDF curve. In the historical period, the judgment of extreme value for the statistical sample and its influence on IDF curve are analyzed. Based on the non-linear relationship for different quantile values of between the model and the observation in the historical period,

the study establishes a solution method for generation of IDF curve in the future period. The conclusions drawn from the study are as follows:

- (i) The optimization accuracy of the parameters of the DRIF by the NSLS algorithm is the best. In the historical period of Beijing, the variation range of the rainstorm intensity of different durations for the 100-year return period is 0.169–4.124 mm/min;
- (ii) For the processing of this outlier, the Z-Score was recommended to judge the outlier in this study. The best alternative to the outlier is the AVG method, which takes the average of the series in the sample that are larger than the critical value. The error of SMV in the high return period is still larger. The rainstorm intensity of MVL in the high return period is obviously smaller. After the outliers are processed, the value of the IDF table is slightly reduced. The percentage of reduction for IDF varies from –0.1 to –3.1%.
- (iii) There is a perfect non-linear relationship between the model and the observation at different quantiles over the historical period. The projected IDF under the four scenarios for this future period are all larger than the observation.
- (iv) Except for the two- and three-year of observation in SSP2-4.5, the return periods of observation in the historical period are all larger than equivalent return periods in future period.

AUTHOR CONTRIBUTIONS

Xingchen Ding: Methodology, Formal analysis, Resources, Writing – original draft, Data curation. **Weihong Liao:** Writing – review. **Hao Wang:** Writing – review. **Hao Wang:** Conceptualization. **Xiaohui Lei:** Supervision. **Jiali Yang:** Supervision, encouragement.

ACKNOWLEDGEMENTS

This study was supported by the National Natural Science Foundation of China (No. 52179027).

DATA AVAILABILITY STATEMENT

Data cannot be made publicly available; readers should contact the corresponding author for details.

CONFLICT OF INTEREST

The authors declare there is no conflict.

REFERENCES

- Asikoglu, O. 2017 Outlier detection in extreme value series. *Journal of Multidisciplinary Engineering Science and Technology* **4**, 7314–7318.
- Bílková, D. 2012 Lognormal distribution and using L-moment method for estimating its parameters. *International Journal of Mathematical Models and Methods in Applied Sciences* **6** (1), 30–44.
- Butcher, J. B. & Zi, T. 2019 Efficient method for updating IDF curves to future climate projections. arXiv preprint arXiv:1906.04802.
- Chen, B., Zeng, W., Lin, Y. & Zhang, D. 2014 A new local search-based multiobjective optimization algorithm. *IEEE Transactions on Evolutionary Computation* **19** (1), 50–73.
- Coello, C. C. & Lechuga, M. S. 2002 MOPSO: A Proposal for Multiple Objective Particle Swarm Optimization. IEEE, Honolulu, USA, pp. 1051–1056.
- Crosby, T. 1995 How to detect and handle outliers. *Technometrics* **36**, 315–316.
- Deb, K., Pratap, A., Agarwal, S. & Meyarivan, T. 2002 A fast and elitist multiobjective genetic algorithm: NSGA-II. *IEEE Transactions on Evolutionary Computation* **6** (2), 182–197.
- Doi, M. V. & Kim, J. 2021 Addressing climate internal variability on future intensity-duration-frequency curves at fine scales across South Korea. *Water-Sui* **13** (20), 2828.
- Dong, T. & Dong, W. 2021 Evaluation of extreme precipitation over Asia in CMIP6 models. *Climate Dynamics* **57** (7), 1751–1769.
- Fadhel, S., Rico-Ramirez, M. A. & Han, D. 2017 Uncertainty of intensity–duration–frequency (IDF) curves due to varied climate baseline periods. *Journal of Hydrology* **547**, 600–612.
- Grubbs, F. E. 1969 Procedures for detecting outlying observations in samples. *Technometrics* **11** (1), 1–21.

- Grubbs, F. E. & Beck, G. 1972 Extension of sample sizes and percentage points for significance tests of outlying observations. *Technometrics* **14** (4), 847–854.
- Guo, H., Bao, A., Chen, T., Zheng, G., Wang, Y., Jiang, L. & De Maeyer, P. 2021 Assessment of CMIP6 in simulating precipitation over arid Central Asia. *Atmospheric Research* **252**, 105451.
- Huang, Z., Xie, Z., Zhang, C., Chan, S. H., Milewski, J., Xie, Y., Yang, Y. & Hu, X. 2019 Modeling and multi-objective optimization of a stand-alone PV-hydrogen-retired EV battery hybrid energy system. *Energy Conversion and Management* **181**, 80–92.
- Jia, P., Zhuang, D. & Wang, Y. 2017 Impacts of temperature and precipitation on the spatiotemporal distribution of water resources in Chinese mega cities: the case of Beijing. *Journal of Water and Climate Change* **8** (4), 593–612.
- Kannan, K. S., Manoj, K. & Arumugam, S. 2015 Labeling methods for identifying outliers. *International Journal of Statistics and Systems* **10** (2), 231–238.
- Kotz, S. & Nadarajah, S. 2000 *Extreme Value Distributions: Theory and Applications*: Imperial College Press, London.
- Lu, T. & Cui, X. 2022 Observational comparison of Two torrential rainfall events in Beijing. *Chinese Journal of Atmospheric Sciences* **46** (1), 111–132.
- Lu, Y., Kumar, J., Collier, N., Krishna, B. & Langston, M. A. 2018 *Detecting Outliers in Streaming Time Series Data From ARM Distributed Sensors*. IEEE, USA, pp. 779–786.
- Mailhot, A., Duchesne, S., Caya, D. & Talbot, G. 2007 Assessment of future change in intensity–duration–frequency (IDF) curves for Southern Quebec using the Canadian regional climate model (CRCM). *Journal of Hydrology* **347** (1–2), 197–210.
- Mirhosseini, G., Srivastava, P. & Stefanova, L. 2013 The impact of climate change on rainfall intensity–Duration–Frequency (IDF) curves in Alabama. *Regional Environmental Change* **13** (1), 25–33.
- Pachauri, R. K., Allen, M. R., Barros, V. R., Broome, J., Cramer, W., Christ, R., Church, J. A., Clarke, L., Dahe, Q. & Dasgupta, P. 2014 *Climate Change 2014: Synthesis Report. Contribution of Working Groups I, II and III to the Fifth Assessment Report of the Intergovernmental Panel on Climate Change*. IPCC, Geneva, Switzerland.
- Peng, L. & Li, Z. 2021 Ensemble flood risk assessment in the Yangtze River economic belt under CMIP6 SSP-RCP scenarios. *Sustainability-Basel* **13** (21), 12097.
- Ren, M., Xu, Z., Pang, B., Liu, W., Liu, J., Du, L. & Wang, R. 2018 Assessment of satellite-derived precipitation products for the Beijing region. *Remote Sensing-Basel* **10** (12), 1914.
- Requena, A. I., Nguyen, T., Burn, D. H. & Coulibaly, P. 2021 A temporal downscaling approach for sub-daily gridded extreme rainfall intensity estimation under climate change. *Journal of Hydrology: Regional Studies* **35**, 100811.
- Saleem, S., Aslam, M. & Shaikat, M. R. 2021 A review and empirical comparison of univariate outlier detection methods. *Pakistan Journal of Statistics* **37** (4), 447–462.
- Song, X., Zhang, J., AghaKouchak, A., Roy, S. S., Xuan, Y., Wang, G., He, R., Wang, X. & Liu, C. 2014 Rapid urbanization and changes in spatiotemporal characteristics of precipitation in Beijing metropolitan area. *Journal of Geophysical Research: Atmospheres* **119** (19), 211–250, 271.
- Song, X., Zhang, J., Zhang, C. & Zou, X. 2019 A comprehensive analysis of the changes in precipitation patterns over Beijing during 1960–2012. *Advances in Meteorology* **2019**, 1–22.
- Srivastav, R. K., Schardong, A. & Simonovic, S. P. 2014 Equidistance quantile matching method for updating IDFCurves under climate change. *Water Resources Management* **28** (9), 2539–2562.
- Su, B., Huang, J., Mondal, S. K., Zhai, J., Wang, Y., Wen, S., Gao, M., Lv, Y., Jiang, S. & Jiang, T. 2021 Insight from CMIP6 SSP-RCP scenarios for future drought characteristics in China. *Atmospheric Research* **250**, 105375.
- Tfwala, C. M., Van Rensburg, L. D., Schall, R., Mosia, S. M. & Dlamini, P. 2017 Precipitation intensity-duration-frequency curves and their uncertainties for Ghaap plateau. *Climate Risk Management* **16**, 1–9.
- Tousi, E. G., O'Brien, W., Doulabian, S. & Toosi, A. S. 2021 Climate changes impact on stormwater infrastructure design in Tucson Arizona. *Sustainable Cities and Society* **72**, 103014.
- Ugray, Z., Lasdon, L., Plummer, J., Glover, F., Kelly, J. & Martí, R. 2007 Scatter search and local NLP solvers: a multistart framework for global optimization. *Inform Journal on Computing* **19** (3), 328–340.
- Wan Zin, W. Z., Jemain, A. A. & Ibrahim, K. 2009 The best fitting distribution of annual maximum rainfall in Peninsular Malaysia based on methods of L-moment and LQ-moment. *Theoretical and Applied Climatology* **96** (3), 337–344.
- Xu, C., Sun, Q. & Lu, C. 2022 Analysis of rainfall and temperature characteristics and its correlation with Southern Oscillation Index in Beijing, China. *Water Supply* **22** (4), 4544–4557.
- Yang, P., Ren, G. & Hou, W. 2019 Impact of daytime precipitation duration on urban heat island intensity over Beijing city. *Urban Climate* **28**, 100463.
- Zhang, Q. & Li, H. 2007 MOEA/d: a multiobjective evolutionary algorithm based on decomposition. *IEEE Transactions on Evolutionary Computation* **11** (6), 712–731.
- Zhang, H., Niu, K., Wang, J. & Wang, N. 2016 Improved MOPSO algorithm based on map-reduce model in cloud resource scheduling. *Journal of Computers* **27** (2), 67–78.
- Zhang, Y., You, Q., Chen, C., Ge, J. & Adnan, M. 2018 Evaluation of downscaled CMIP5 coupled with VIC model for flash drought simulation in a humid subtropical basin, China. *Journal of Climate* **31** (3), 1075–1090.

- Zhang, Q., Zhang, L., Deng, Y., Wang, S. & Xiao, Y. 2021 The research progress and prospects of climate model and hydrological simulation key technology. *Advances in Meteorological Science and Technology* **3** (11), 126–134.
- Zhao, D. G. & Li, Q. 2014 *Optimization of Vehicle-Borne Radar Antenna Pedestal Based on Modified NSGA-II*. Trans Tech Publ, Switzerland, pp. 2241–2247.
- Zhou, Q., Leng, G. & Huang, M. 2018 [Impacts of future climate change on urban flood volumes in Hohhot in northern China: benefits of climate change mitigation and adaptations](#). *Hydrology and Earth System Sciences* **22** (1), 305–316.

First received 7 June 2022; accepted in revised form 4 August 2022. Available online 8 August 2022